An et al., Int J Metall Mater Eng 2016, 2: 124
http://dx.doi.org/10.15344/2455-2372/2016/124

International Journal of
Metallurgical & Materials Engineering

Research Article Open Access

Thermodynamic and Kinetic Properties of $La_{20.5}MgNi_{78.5}$ and $La_{15.5}Mg_6Ni_{78.5}$ Hydrogen Storage Alloys: The Theoretical Models and Their Verifications

Xue-Hui An[1], Yuepeng Pang[1], Qin Li[1], Jie-Yu Zhang[1], Kuo-Chih Chou[1], Qian Li[1,2*]

[1]*State Key Laboratory of Advanced Special Steels & Shanghai Key Laboratory of Advanced Ferrometallurgy & School of Materials Science and Engineering, Shanghai University, Shanghai 200072, China*

[2]*Materials Genome Institute, Shanghai University, Shanghai 200444, China*

Abstract

In this paper, we present a statistic thermodynamic model quantitatively describing the pressure-composition-isotherms (PCI) curve, which consists of hydrogen storage capacity, temperature, and equilibrium pressure in the hydriding and dehydriding (H/D) reactions, and a theoretical kinetic model to clarify the H/D kinetic mechanism of hydrogen storage alloys. The results of the calculations are well agreed with the experiments performed with $La_{20.5}MgNi_{78.5}$ and $La1_{5.5}Mg_6Ni_{78.5}$ alloys, their maximum hydrogen storage capacities and the hydride formation enthalpies at 303~333 K are 1.41 wt.% H_2 and -31.64 kJ/mol H_2 for $La_{20.5}MgNi_{78.5}$ and 1.31 wt.% H_2 and -27.23 kJ/mol H_2 for $La1_{5.5}Mg_6Ni_{78.5}$, respectively. A new diffusion kinetic model is proposed with the consideration of Pilling–Bedworth Ratio, i.e. hydrogen-induced volume change used for studying the hydrogen absorption reaction kinetics. The activation energies are calculated to be 31.25 kJ/mol H_2 for $La_{20.5}MgNi_{78.5}$ and 24.24 kJ/mol H_2 for $La1_{5.5}Mg_6Ni_{78.5}$, respectively.

Publication History:
Received: May 25, 2016
Accepted: June 28, 2016
Published: June 30, 2016

Keywords:

Hydrogen storage alloys, Thermodynamic and kinetic properties, Theoretical model, Experimental verification

Introduction

Due to their potential for practical application, hydrogen storage properties of alloys in the Ni-rich corner of the La–Mg–Ni ternary system were extensively studied, such as $CaCu_5$–type $LaNi_5$ (AB_5), $PuNi_3$-type $(La,Mg)Ni_3$, Ce_2Ni_7-type $(La,Mg)_2Ni_7$, and Pr_5Co_{19}-type $(La,Mg)_5Ni_{19}$ [1–3]. These alloys that have layer structure of $[LaMgNi_4]$ and $[LaNi_5]$ units alternatively stacking along c axis [4–6] were expected to have the comprehensive properties of the AB_2-type and AB_5-type alloys, i.e. large hydrogen storage capacity and fast hydriding/dehydriding (H/D) reaction rates. For example, Nakamura et al. [6] identified that the La_4MgNi_{19} transformed to $La_4MgNi_{19}H_{24}$ after absorbing hydrogen by in-situ X-ray diffraction and neutron powder diffraction. Férey et al. [7] concluded that the La_4MgNi_{19} exhibited a much higher reversible hydrogen storage capacity than La_5Ni_{19}. Liu et al. [8] reported that $(La,Mg)_5Ni_{19}$ multiphase alloy showed a good cyclic stability and 89% hydrogen capacity remained within 30 H/D cycles under 5 MPa. Kadir et al. [9] first identified that the $LaMg_2Ni_9$ alloy had layer structure stacking from the $MgNi_2$ Laves-type alternating with $LaNi_5$ layers. Denys et al. [10] reported that the reversible hydrogen storage capacities of $La_{3-x}Mg_xNi_9$ (x=0~0.67) increased with the rise of Mg content. The hydrogen storage capacity of $LaMg_2Ni_9$ was 0.33 wt.% H/M at 303 K under 3.3 MPa H_2 [11]. Liu et al. [12] improved the cycling stability and the maximum high rate dischargeability of $La_{0.75}Mg_{0.25}Ni_{3.5}$ by annealing treatment.

The theoretical model is one of the most useful methods for studying the hydrogen storage properties, including the PCI curves and the kinetics, which are keys for application. Assuming that the metal-hydrogen system was univariant, Lacher et al. [13] interpreted the PCI curve of Pd–H system. Later, Beeri et al. [14–16] revised the Lacher-type model by applying Bragg-Williams and the Quasi-Chemical approximations and derived the PCI curves, considering the situations of real gas and the existence of multiple plateaus. Senoh et al. [17] interpreted the PCI curves theoretically based on statistical mechanics, in which the RNi_5 (R = La, Pr, Nd and Sm)–H was regarded as a grand canonical ensemble. Lexcellent et al. [18] modeled the anhysteretic PCI curves, discussed the plateau or slope in detail, and finally applied it in the La–Ni-based alloys. Ledovskikh et al. [19] divided the PCI curves into three parts and derived their theoretical models individually by adopting the macroscopic thermodynamic equation and statistical theory of entropy. Unfortunately, the models cannot work well in the La–Mg–Ni ternary system.

As the kinetic models describing the H/D reactions are concerned, numerous models were proposed to elucidate the mechanism of the gas-solid kinetics for hydrogen storage materials. The 41 typical kinetic models were summarized in Ref. [20], among which the Jander model and Johnson–Mehl–Arvami (JMA) model were usually used to describe the H/D kinetics [21, 22]. Many other models were reported, for example, on the basis of shrinking core model, Smith et al. [23] deduced a model for describing the kinetics of the $LaNi_{5-x}Co_x$, in which the chemical reaction at the α–β interface was likely the rate-controlling step. Blanco et al. [24] supposed that only one step controlled the hydrogen absorption reaction, with other steps in the equilibrium state. They gave out the kinetic expressions of each controlling step and applied them to the La–Ni–Sn system. In recent years, Chou et al. [25, 26] introduced the concept of characteristic time and proposed a new kinetic model which described the kinetics of different hydrogen storage alloy systems quite well [27–29]. Later, Chou also proposed a new model to describe the isothermal oxidation of metals and alloys in the form of sphere, flat plate and fiber shape with considering oxidation induced volume change [30].

In this work, on the basis of the more realistic physical assumptions, a model for PCI curves from the view of thermodynamic statistic as well as a kinetic model with the consideration of hydrogen-induced volume change is proposed for describing the hydrogen storage properties. The results of the models are compared with measurements

***Corresponding Author:** Dr. Qian Li, State Key Laboratory of Advanced Special Steels & Shanghai Key Laboratory of Advanced Ferrometallurgy & School of Materials Science and Engineering, Shanghai University, Shanghai 200072, China; E-mail: shuliqian@shu.edu.cn

Citation: An XH, Pang Y, Li Q, Zhang JY, Chou KC, et al. (2016) Thermodynamic and Kinetic Properties of $La_{20.5}MgNi_{78.5}$ and $La_{15.5}Mg_6Ni_{78.5}$ Hydrogen Storage Alloys: The Theoretical Models and Their Verifications. Int J Metall Mater Eng 2: 124. doi: http://dx.doi.org/10.15344/2455-2372/2016/124

on $La_{20.5}MgNi_{78.5}$ and $La1_{5.5}Mg_6Ni_{78.5}$ alloys, which are selected according to the updated La–Mg–Ni phase diagram in our previous work [31].

Theoretical and Experimental Description

Statistic thermodynamic model

Based on the statistical thermodynamic theory, the present paper divides the PCI curve into three parts, i.e., α, α+β and β regions. It concerns the fugacity factor of real gas and proposes a new model to interpret the PCI curve. The derivation is summarized as follows.

The present paper adopts the hypothesis of Ledovskikh et al. [19], assuming that a hydrogen storage alloy particle consists of M unit cell, and each unit cell have d host sites. Therefore, the total number of vacancies (N) and H atoms (n) for the α, α+β and β regions can be expressed as

$$N_\alpha = \begin{cases} d_\alpha M \\ d_\alpha M \dfrac{x_\beta - x}{x_\beta - x_\alpha} \\ 0 \end{cases} \quad N_\beta = \begin{cases} 0 & x < x_\alpha \\ d_\beta M \dfrac{x - x_\alpha}{x_\beta - x_\alpha} & x_\alpha \le x \le x_\beta \\ d_\beta M & x > x_\beta \end{cases} \quad (1)$$

$$n_\alpha = n_{\max} \begin{cases} x \\ x_\alpha \dfrac{x_\beta - x}{x_\beta - x_\alpha} \\ 0 \end{cases} \quad n_\beta = n_{\max} \begin{cases} 0 & x < x_\alpha \\ x_\beta \dfrac{x - x_\alpha}{x_\beta - x_\alpha} & x_\alpha \le x \le x_\beta \\ x & x > x_\beta \end{cases} \quad (2)$$

where n_{max} is the maximum number of the H atoms, n_α and n_β are the number of the H atoms in the α and β phases respectively, x_α and x_β stand for the fraction of H atoms in the α and β phases respectively, d_α and d_β represent the host sites per unit cell in the α and β phases respectively, generally $d_\beta \ge d_\alpha$. The structures of $LaNi_5$, $LaMg_2Ni_9$ and La_4MgNi_{19} are hexagonal before and after hydrogen absorption, therefore, $d=d_\beta/d_\alpha=1$. The footnotes of α and β represent the parameters in α and β phases, respectively.

According to the Bragg-Williams approximation, the H atoms occupy the vacancy randomly. The energy for hydrogenation process consists three parts [19], the energy of absorbed hydrogen in the α phase and β phase, represented by E_α and E_β, respectively; the interactive energy between the two H atoms in the α phase ($\chi_{\alpha\alpha}$), β phase ($\chi_{\beta\beta}$) and α+β phases ($\chi_{\alpha\beta}$); and the contribution of each unit cell to the total energy for the α and β phases, denoted as L_α and L_β, respectively. Based on the mean-field approximation, the Hamiltonian (U) of the entire system is expressed as Eq. (3)

$$U = L_\alpha M_\alpha + L_\beta M_\beta + E_\alpha n_\alpha + E_\beta n_\beta + \frac{\chi_\alpha}{2}\frac{n_\alpha^2}{n_{\max}} + \frac{\chi_\beta}{2}\frac{n_\beta^2}{n_{\max}} + \frac{\chi_\beta}{2}\frac{n_\alpha n_\beta}{n_{\max}} \quad (3)$$

Further, the partition function (Ω) is written as

$$\Omega = \frac{N_i!}{n_i!(N_i - n_i)!} e^{-\frac{U}{kT}} \quad (4)$$

Each point on the PCI curves was under the equilibrium state and the volume of sample holder didn't change during the measurement. Therefore, the Helmholtz energy is adopted to descript the energy change, as Eq. (5)

$$A = -kT \ln \Omega \quad (5)$$

where K is the Boltzmann constant. According to the Stirling approximation, Eq. (5) can be written as

$$A = U + kTN_i\left[\frac{n_i}{N_i}\mathrm{h}\ \frac{n_i}{N_i} + \left(1 - \frac{n_i}{N_i}\right)\mathrm{h}\left(1 - \frac{n_i}{N_i}\right)\right] \quad (6)$$

Since the PCI measurement is regarded as at the equilibrium state, the chemical potentials of H in the metal and gas are equal. Therefore,

$$\mu_{(\mathrm{H/M})} = \frac{\partial \mathrm{A}}{\partial n} = \frac{1}{2}\mu_{(H_2)} \quad (7)$$

where $\mu_{(H/M)}$ and $\mu_{(H_2)}$ are the chemical potentials of the H atom in the alloy and H_2 in the gas, respectively.

As for α, α+β and β, the chemical potential of H atom in the metal can be express as:

$$\mu_{(H/M)} = E_\alpha + \chi_{\alpha\alpha}x + kT\ln\frac{xd}{1-xd} \qquad (x<x_\alpha) \quad (8)$$

$$\mu_{(H/M)} = \left[\frac{L}{x_\beta - x_\alpha} - \frac{E_\alpha x_\alpha}{x_\beta - x_\alpha} + \frac{E_\beta x_\beta}{x_\beta - x_\alpha} - \frac{\chi_{\alpha\alpha}x_\alpha^2}{x_\beta - x_\alpha}\left(\frac{x_\beta - x}{x_\beta - x_\alpha}\right) + \frac{\chi_{\beta\beta}x_\beta^2}{x_\beta - x_\alpha}\left(\frac{x - x_\alpha}{x_\beta - x_\alpha}\right) + \frac{\chi_{\alpha\beta}x_\alpha x_\beta}{(x_\beta - x_\alpha)^2}(x_\beta - 2x + x_\alpha)\right] - kT\frac{S_\alpha^0/d - S_\beta^0}{x_\beta - x_\alpha} \quad (\mathrm{x}\alpha \le \mathrm{x} \le \mathrm{x}\beta)$$

$$\mu_{(H/M)} = E_\beta + \chi_{\beta\beta}x + kT\ln\frac{x}{1-x}$$

The chemical potential of H_2 under a high pressure is written as Eq. (9)

$$\mu_{(H_2)} = \frac{1}{2}\left(\mu^\circ{}_{(H_2)} + \varepsilon kT \ln P/P^\circ\right) \quad (9)$$

where P° is the standard pressure, at the value of 10^5 Pa;

, $\mu^\circ_{(H_2)} = kT \times C(T) - D_0$ and D_0 is a constant of 7.17 J/molecule,

$$C(T) = 7.78 - 3.5 \times \ln(T) + \ln\left[1 - \exp\left(-\frac{6240}{T}\right)\right] \quad \varepsilon \approx 1 + \frac{1}{\ln(P)}\int_0^P [Z(P,T) - 1]\frac{dP}{P}$$

$Z(P,T) = 1 + \sum_{i=1}^{m} \frac{a_i(T)}{V_i(P)}$ $a_i(T)$ the Virial coefficient of high pressure gas; $Z(P,T)$ is the compressibility of high pressure gas; $V_i(P)$ is the mole volume.

Therefore, the PCI curves can be described by the following equations,

For the α phase region:

$$P = P^\circ \exp\frac{1}{\varepsilon}\left[\frac{2(E_\alpha + \chi_{\alpha\alpha}x) + D_0}{kT} + 2\ln\left(\frac{xd}{1-xd}\right) - C(T)\right] \quad (10)$$

For the mixing of α and β phase region:

$$P = P^\circ \exp\frac{2}{\varepsilon kT}\left\{\frac{L}{x_\beta - x_\alpha} - \frac{E_\alpha x_\alpha}{x_\beta - x_\alpha} + \frac{E_\beta x_\beta}{x_\beta - x_\alpha} - \frac{\chi_{\alpha\alpha}x_\alpha^2}{x_\beta - x_\alpha}\left(\frac{x_\beta - x}{x_\beta - x_\alpha}\right) + \frac{\chi_{\beta\beta}x_\beta^2}{x_\beta - x_\alpha}\left(\frac{x - x_\alpha}{x_\beta - x_\alpha}\right) + \frac{\chi_{\alpha\beta}x_\alpha x_\beta}{(x_\beta - x_\alpha)^2}(x_\beta - 2x + x_\alpha) - \frac{(S_\alpha^\circ/d - S_\beta^\circ)kT}{x_\beta - x_\alpha} - \frac{1}{2}kTC(T) + \frac{D_0}{2}\right\} \quad (11)$$

For the β phase region:

$$P = P^\circ \exp\frac{1}{\varepsilon}\left[\frac{2(E_\beta + \chi_{\beta\beta}x) + D_0}{kT} + 2\ln\left(\frac{x}{1-x}\right) - C(T)\right] \quad (12)$$

where x_α, x_β, E_α, E_β, $\chi_{\alpha\alpha}$, $\chi_{\beta\beta}$, $\chi_{\alpha\beta}$ are the parameters to be calculated using the Eqs.(10)–(12);

$$L = D_{\alpha\beta} - E_\beta x_\beta + E_\alpha x_\alpha + \frac{\chi_{\alpha\alpha}x_\alpha^2 - \chi_{\beta\beta}x_\beta^2}{2} - \left[D_\alpha + D_\beta - \left(E_\alpha + E_\beta\right) - \left(\chi_{\alpha\alpha}x_\alpha + \chi_{\beta\beta}x_\beta\right)\right]\frac{x_\beta - x_\alpha}{2}$$

$$\chi_{\alpha\beta} = \frac{\chi_{\alpha\alpha}x_\alpha^2 + \chi_{\beta\beta}x_\beta^2}{x_\alpha x_\beta} - \frac{D_\alpha - D_\beta - E_\alpha + E_\beta - \chi_{\alpha\alpha}x_\alpha + \chi_{\beta\beta}x_\beta}{x_\alpha x_\beta}\left(x_\beta - x_\alpha\right)$$

$$D_{\alpha\beta} = kT\left(\frac{S_\alpha^0}{d} - S_\beta^0\right) D_\alpha = kT\left(\frac{1 - x_\alpha d}{x_\alpha d}\right) D_\beta = kT\left(\frac{1 - x_\beta}{x_\beta}\right)$$

Kinetic model

Great deals of models were reported for the description of the kinetics of the H/D processes in the past years. In recent years, Chou model was provided to describe and predict the kinetic mechanism of the gas-solid reaction, including physisorption, chemisorption, surface penetration, diffusion of hydrogen atoms in hydride and chemical reaction. In most cases, the diffusion and surface penetration are the rate-controlling steps [25, 26], and they have been successfully applied in many hydrogen storage alloys [27–29]. Actually, the alloy particle volume will be increased after hydrogenation reaction, compared with the gas-solid reaction in oxidation of metal and alloy, the technique word of "the difference between the volumes of matrix and oxide layer" can be expressed as the Pilling–Bedworth Ratio, which was firstly noticed by Pilling and Bedworth in 1923 [32]. Therefore, we take account of hydrogen-induced volume change, i.e. Pilling–Bedworth Ratio, and propose a new kinetic model in the present work. Assuming that the hydrogen atoms diffuse through the hydride product layers stably, then the rate-controlling step is diffusion; the hydrogen storage alloy particles are spheres with the same density and diameters; the hydriding reaction proceeds from the outer to the inner and the hydride layers are continuous with metal and hydride contacting completely.

Define that the R_{PB} is the ratio of the hydride volume and the unreacted metal volume, expressed as

$$R_{PB} = \eta = V_{hydride}/V_{unreacted\ metal},$$

$$\eta = \frac{V_{hydride}}{V_{unreactedmetal}} = \frac{M_\beta n_\beta}{\rho_\beta} \Big/ \frac{M_m n_m}{\rho_m} = \frac{M_\beta n_\beta}{\rho_\beta}\frac{\rho_m}{M_m n_m} \quad (13)$$

where η is Pilling–Bedworth Ratio; M_β and ρ_β are the amount and the density of the hydride; $V_{hydride}$ is the volume of the hydride produced by the reaction; $V_{unreacted\ metal}$ is the volume of the unreacted hydrogen storage alloy particles.

Based on the diffusion expression of the Chou model and Valensi-Carter model [25, 26, 33], the kinetics can be expressed as Eq. (14).

$$\left[1 + (\eta - 1)\xi\right]^{\frac{2}{3}} + (\eta - 1)(1 - \xi)^{\frac{2}{3}} - \eta = \frac{1}{\gamma}\frac{M_m}{\rho_m}\frac{2(\eta - 1)}{r_0^2} D_H^0 K_H^0 \exp\left(-\frac{\Delta\varepsilon + \Delta H}{RT}\right)\left(\sqrt{P_{eq}} - \sqrt{P_{H2}}\right)t \quad (14)$$

where $\eta \neq 1$. ξ is the reacted fraction of absorbed hydrogen; t is the reacted time; T is the reacted temperature; D_H^0 and K_H^0 are the constants independent of T; $\Delta\varepsilon$ is the activated energy of hydrogen atom passing through the hydride layer; P_{H2} is the partial hydrogen pressure in gas/hydride; P_{eq} is the equilibrium pressure; ΔH is the reaction enthalpy of hydrogen dissolution.

Characteristic time (t_c) was first proposed by Chou et al. [25, 26], whose physical meaning is the required time to complete the hydriding reaction. So define

$$t_c = \frac{\eta^{\frac{2}{3}} - \eta}{\frac{1}{\gamma}\frac{M_m}{\rho_m}\frac{2(\eta - 1)}{r_0^2} D_H^0 K_H^0 \exp\left(-\frac{\Delta\varepsilon + \Delta H}{RT}\right)\left(\sqrt{P_{eq}} - \sqrt{P_{H2}}\right)} \quad (15)$$

Substituting Eq. (15) into Eq. (14), the Eq. (16) is obtained.

$$(\eta - 1)(1 - \xi)^{\frac{2}{3}} + \left[1 + (\eta - 1)\xi\right]^{\frac{2}{3}} - \eta = \frac{\eta^{\frac{2}{3}} - \eta}{t_c}t \quad (16)$$

When $t = t_c$, $\xi = 1$. So the smaller value of t_c is, the faster the reaction rate will be.

In the Chou model, when diffusion is the rate-controlling step, the expression is

$$\xi = 1 - \left(1 - \sqrt{t/t_c}\right)^3 \quad (17)$$

From Eq. (17), ξ is larger than 1 after the reaction is completed, i.e. $t > t_c$, $\xi > 1$, which deviates from the actual experimental results.

According to Eq. (14),

$$\xi'' = -\frac{3K'^2(C_e - C_0)^2}{r_0^4}\frac{\eta(1 - \xi)^{-\frac{4}{3}}}{\left\{(1 - \xi)^{-\frac{1}{3}} - \left[1 + \xi(\eta - 1)\right]^{-\frac{1}{3}}\right\}^3} \quad (18)$$

If $\xi''=1$. $\xi=1$ From Eq. (18), it can be seen that when $\xi''<0$, $\xi \neq 1$. Therefore, $\xi = 1$ is not the inflexion of Eq. (18), which indicates that there is no inflexion in the curve. Obviously, the modified model not only considers the RPB, but also describes the experimental results more accurately.

Experimental details

According to the thermodynamic description of the La–Mg–Ni system [31], two alloys, composition very close to nominal $La_{20.5}MgNi_{78.5}$ (labeled as sample #1) and $La1_{5.5}Mg_6Ni_{78.5}$ (labeled as sample #2), locating at the $LaNi_5$ & $(La,Mg)_5Ni_{19}$ and $LaNi_5$ & $(La,Mg)Ni_3$ binary zone, were selected and synthesized from the bulk of La (99.99 %), Mg (99.99 %), and Ni (99.999 %) using a medium frequency induction furnace. Before melting, the induction furnace was vacuumed to lower than 10 Pa and then injected with high purity argon (99.999 %) to 0.1 MPa. It is difficult to control the content of Mg in the alloy due to its evaporable property. In order to reach the target composition, we melt the alloys by the following steps. First, melt the refined La and Ni together at around 1600 K to make master alloy in a copper crucible which was cooled by the cooling water for the whole melting process. Second, put the Mg and master alloy together, melt them and weight the finished alloy. If the weight of finished alloy was lower than the weight of target alloy, we would add more Mg based on its burning loss rate and remelt the alloy. Contrarily, if the final weight is larger than the target alloy, the alloy should be kept at high temperature for Mg evaporation to the target weight. In order to make the composition more uniform, we turn around the melt at least three times during the melting process. The composition of target alloys was analyzed by Optima 7300DV ICP. The actual compositions are $La1_{9.90}Mg_{1.79}Ni_{78.31}$ and $La_{15.14}Mg_{6.30}Ni_{78.56,}$ respectively, close to their nominal composition.

The finished alloys were grinded into powder of ~300 mesh in a glove box for the XRD analysis. The XRD measurements were carried out on a DLMAX–2200 diffractometer (CuK_α radiation, $10° \le 2\theta \le 90°$, 2°/min) operated at 40 kV and 40 mA. The Materials Data Inc. software Jade 5.0 and a Powder Diffraction File database were used to analyze the XRD patterns for phase identification.

Diffraction File database were used to analyze the XRD patterns for phase identification.

As for the H/D analysis, the target alloys were also grinded into powder of ~200 mesh in a glove box. About 1.5 g alloy powders were set in a volume calibrated sample holder. The powders were fully activated by repeated hydriding at 363 K under 4MPa H_2 for 30 min and dehydriding at 303 K in vacuum of 10 Pa for 30 min for ten times. The PCI curves and kinetics were investigated by a Sieverts type volumetric equipment under high purity hydrogen (99.999%) atmosphere at 303, 318 and 333 K after completed activation. The hydriding reaction rates were measured under 2 MPa H_2 at the same temperature controlled by a thermostat water bath.

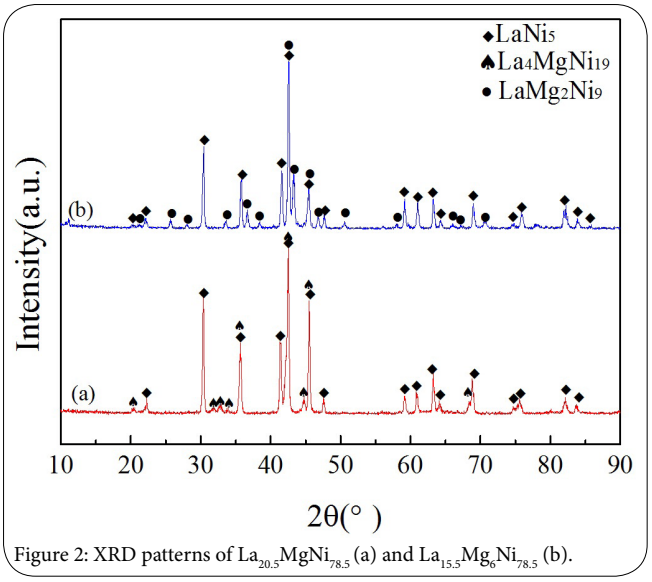

Figure 2: XRD patterns of $La_{20.5}MgNi_{78.5}$ (a) and $La_{15.5}Mg_6Ni_{78.5}$ (b).

Results and Discussion

The PCI curves of samples #1 and #2 at 303, 318 and 333K are shown in Figure 1, from which it can be seen that the maximum hydrogen storage capacity of sample #1 (1.41 wt.%H_2) is larger than that of sample #2 (1.31 wt.%H_2). According to the updated La–Mg–Ni phase diagram [31], sample #1 is composed of $LaNi_5$ and La_4MgNi_{19}, and sample #2 contains $LaNi_5$ and $LaMg_2Ni_9$. As can be seen in Figure 2, the results of XRD patterns are agreed with the calculated phase diagram. However, only one plateau is observed in Figure1(a), and Figure 1(b). From Figure 2, the amount of $LaNi_5$ is obviously larger than those of La_4MgNi_{19} and $LaMg_2Ni_9$ for both sample #1 and sample #2, respectively. Moreover, the plateau pressure of $LaNi_5$ is closed to those of La_4MgNi_{19} and $LaMg_2Ni_9$, the plateau pressures of the La_4MgNi_{19} and $LaMg_2Ni_9$ are 0.1 MPa at 298 K [9] and 0.3 MPa at 303 K [10], respectively. So it is difficult to distinguish their plateaus from the PCI curves.

The Eqs. (10)–(12) are used to describe the PCI behaviors of the H/D process of the two samples. The PCI curve is divided into three parts and nonlinearly calculated with Eqs. (10)–(12) by least-squares method, respectively. The calculated results are demonstrated as solid lines in Figure 3. All the calculated results have a good consistent with the experimental data, and the r^2 values of the nonlinear regression equations are all larger than 0.99. Values for the energy of absorbed hydrogen, the interactive energy between the two H atoms and the contribution of each unit cell to the total energy in the according phase are calculated and listed in Table 1.

The parameters of x_α and x_β represent the end point of the plateau, the difference between x_β and x_α represent the length of the plateau, which is another characteristic and property for evaluating the performance of hydrogen storage alloys. Further, the pressure at the middle point of the plateau (P_m) obtained from Eq. (11) is used to calculate the formation enthalpies (ΔH) and entropies (ΔS) of the hydride by Van't Hoff equation. The values of x_α, x_β, x_β-x_α, P_m, ΔH and ΔS are also listed in Table 1. The hydrogen absorption enthalpies of the sample #1 and sample #2 are –31.64 kJ/mol H_2 and –27.23 kJ/mol H_2, respectively; while the hydrogen desorption enthalpies are 35.02 kJ/mol H_2 and 31.39 kJ/mol H_2, respectively. In Table 1, it can be found that the plateau length of sample #1 is shorter than that of

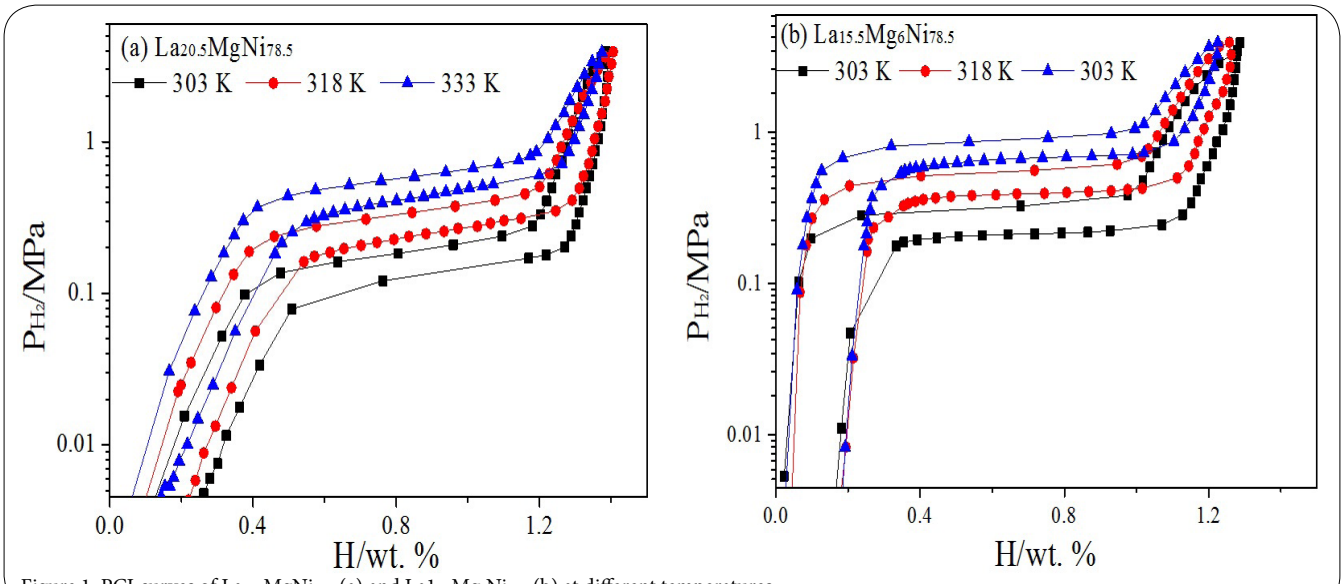

Figure 1: PCI curves of $La_{20.5}MgNi_{78.5}$ (a) and $La1_{5.5}Mg_6Ni_{78.5}$ (b) at different temperatures.

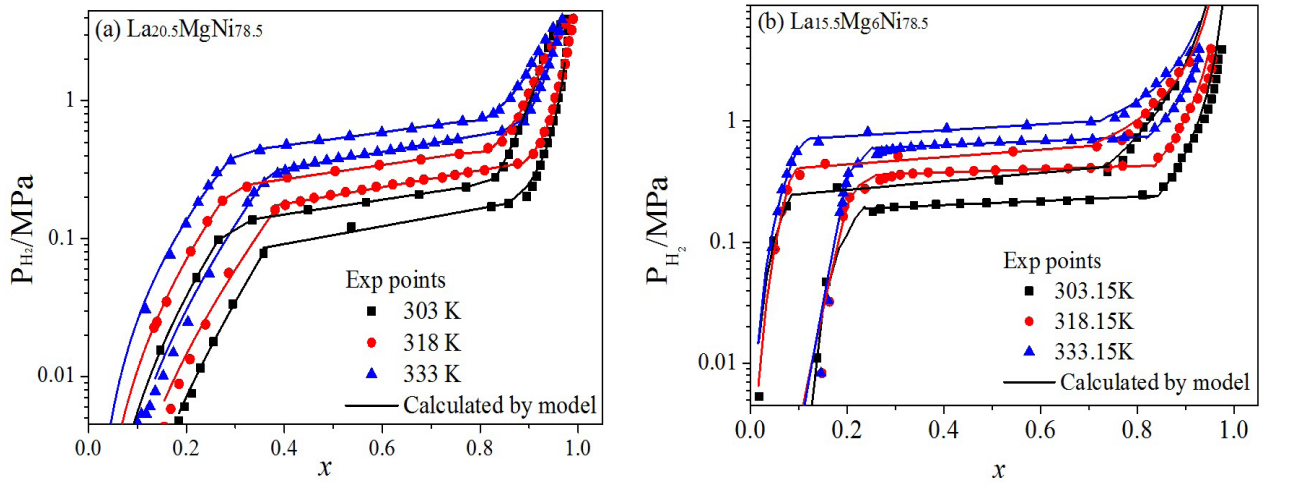

Figure 3: A comparison between the calculated PCI curve (solid lines) and their experimental data (points) for $La_{20.5}MgNi_{78.5}$ (a) and $La_{15.5}Mg_6Ni_{78.5}$ (b) at different temperatures.

Samples	Process	T(K)	E_α(eV)	E_β(eV)	χ_α(eV)	χ_β(eV)	$\chi_{\alpha\beta}$(eV)	L(eV)	x_α	x_β	x_β- x_α	P_m(Mpa)	ΔH(kJ/mol)	ΔS(J/K/mol)
$La_{20.5}MgNi_{78.5}$	Absorption	303	0.0155	−0.0366	0.0409	0.00985	0.0277	0.0336	0.287	0.826	0.539	0.1814	−31.64	−109.30
		318	0.0270	0.0431	0.0313	−0.0785	−0.2176	0.0051	0.292	0.821	0.530	0.3248		
		333	0.0428	0.0754	0.0074	−0.1089	−0.2914	−0.0032	0.301	0.810	0.510	0.5622		
	Desorption	303	−0.0116	0.0742	0.0665	−0.1328	−0.2991	−0.0196	0.365	0.865	0.500	0.1257	35.02	117.57
		318	0.0022	0.1207	0.0464	−0.1803	−0.3952	−0.3430	0.389	0.886	0.496	0.2496		
		333	0.0128	0.0839	0.0495	−0.1293	−0.2856	−0.0134	0.372	0.873	0.502	0.4387		
$La1_{5.5}Mg_6Ni_{78.5}$	Absorption	303	0.0830	0.0152	−0.1082	−0.0313	−0.3243	0.0215	0.085	0.733	0.648	0.3195	−27.23	−99.33
		318	0.0730	0.0591	0.1128	−0.0815	−0.6188	0.0080	0.088	0.695	0.607	0.5038		
		333	0.0915	0.0734	−0.0211	−0.0934	−0.5815	0.0075	0.107	0.715	0.608	0.8466		
	Desorption	303	−0.0932	0.0065	0.8130	−0.0462	−0.0544	0.0130	0.175	0.843	0.668	0.2152	31.39	109.97
		318	−0.0243	0.0195	0.3615	−0.0527	−0.1009	0.0148	0.214	0.836	0.622	0.3924		
		333	−0.0387	0.0507	0.4799	−0.0800	−0.1645	0.0030	0.212	0.822	0.610	0.6605		

Table 1: The calculated parameters in statistic thermodynamic model for $La_{20.5}MgNi_{78.5}$ and $La_{15.5}Mg_6Ni_{78.5}$.

sample #2, which might be ascribed to the different properties of La_4MgNi_{19} and $LaMg_2Ni_9$. The hydrogen absorption behavior is well illustrated by the modified Chou model, Eq. (16), as the solid lines shown in Figure 4(a) and Figure 4(b), which show a good consistent with the experimental data. It can also be concluded that, the rate-controlling step in H/D reactions for the two samples is the hydrogen diffusion in hydride. Both the characteristic time and R_{PB} are calculated from the experimental data. With the increasing temperature from 303 to 333 K, the characteristic time of sample #1 rises from 58.42 to 97.70 s, which is corresponding to R_{PB} values of 1.10 and 1.49, while that of sample #2 increases from 38.09 to 91.14 s with R_{PB} growing from 1.70 to 2.56. The characteristic time of sample #1 is larger than that of sample #2, suggesting the sample #1 has a smaller hydrogen absorption rate. Considered the obtained values of RPB, the $La_{15.5}Mg_6Ni_{78.5}$ hydride has a larger volume changes compared with $La_{20.5}MgNi_{78.5}$ alloy after hydrogenation.

On the other hand, one may use another method to clarify the kinetic mechanism of the hydrogen absorption in $La_{20.5}MgNi_{78.5}$ and $La1_{5.5}Mg_6Ni_{78.5}$ through the calculation of activation energy of hydrogen absorption. Define

$$B_T = \frac{1}{\frac{1}{\gamma}\frac{M_m}{\rho_m}\frac{2(\eta-1)}{r_0^2} D_H^0 K_H^0 \left(\sqrt{P_{eq}} - \sqrt{P_{H2}}\right)} \quad (19)$$

Substituting Eq. (19) into Eq. (14), then

$$\left[1+(\eta-1)\xi\right]^{\frac{2}{3}} + (\eta-1)(1-\xi)^{\frac{2}{3}} - \eta = \frac{t}{B_T}\exp\left(-\frac{\Delta\varepsilon}{RT}\right) \quad (20)$$

where $\Delta\varepsilon$ is the activation energy. Generally speaking, $\Delta\varepsilon$ is regarded as a constant at a certain temperature range, B_T as a coefficient.

In the present work, the activation energy is assumed to be a constant at 303~333 K, and then, the experimental data is non-linear fitted using Eq. (20). The predicted results by kinetic model of Eq. (20) were also drawn in Figure 4(a) and Figure 4(b), from which it can be seen that the comparisons between the calculated curves and experimental data of both samples #1 and #2 demonstrate a good agreement with each other. These facts support our model again, which means that the controlling step of absorption in $La_{20.5}MgNi_{78.5}$ and $La_{15.5}Mg_6Ni_{78.5}$ alloys is hydrogen diffusion in the α phase. The activation energy of sample #1 is calculated to be 31.25 kJ/mol H_2,

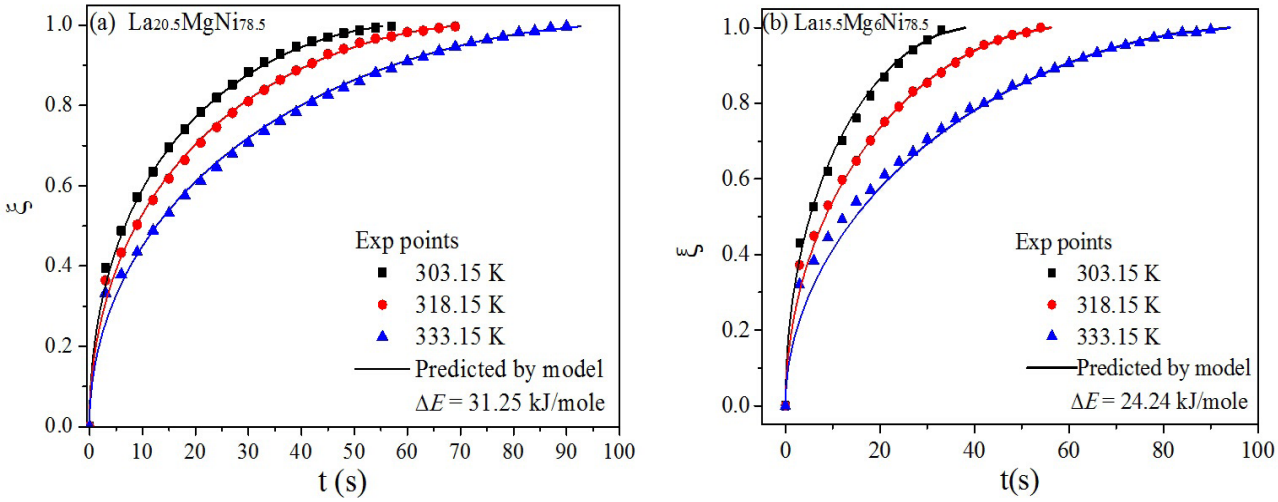

Figure 4: A comparison of transformed fraction (ξ) between experimental data (points) and theoretical prediction (solid lines) for hydrogen absorption in the α phase region for $La_{20.5}MgNi_{78.5}$ (a) and $La1_{5.5}Mg_6Ni_{78.5}$ (b) at different temperatures.

larger than that of sample #2 (24.24 kJ/mol H_2), suggesting that sample #1 has a slower hydriding reaction rate. The results from the activation energy calculation are consistent with the calculation for characteristic time.

Conclusion

On the basis of the more realistic physical assumptions, a model for PCI curves from the view of thermodynamic statistic as well as a kinetic model with the consideration of hydrogen-induced volume change are proposed for describing the hydrogen storage properties. The calculations of the models are compared with measurements on $La_{20.5}MgNi_{78.5}$ and $La_{15.5}Mg_6Ni_{78.5}$ alloys and present a good consistent with experimental data. The H/D enthalpies of the sample #1 are –31.64 kJ/mol H_2 and 35.02 kJ/mol H_2, while for sample #2, they are –27.23 kJ/mol H_2 and 31.39 kJ/mol H_2, respectively. A modified Chou model is deduced on the account of hydrogen-induced volume change. The hydrogenation activation energies are calculated to be 31.25 and 24.24 kJ/mol H_2 for samples #1 and #2, respectively. The results indicate that the hydrogen diffusion in the α phase is the controlling step of absorption in $La_{20.5}MgNi_{78.5}$ and $La_{15.5}Mg_6Ni_{78.5}$ alloys.

Competing Interests

The author(s) have declared that no competing interests exist.

Acknowledgements

The authors gratefully acknowledge support for materials analysis and research from Instrumental Analysis and Research Center of Shanghai University.

Funding

This work was financially sponsored by the Natural Science Foundation of China (No. 51501107, 51222402), "Shu Guang" project supported by Shanghai Municipal Education Commission and Shanghai Education Development Foundation (13SG39) and China Postdoctoral Science Foundation (2015M571541).

References

1. Wang BP, Zhao LM, Cai CB, Wang SX (2014) Effects of surface coating with polyaniline on electrochemical properties of La–Mg–Ni-based electrode alloys. Int J Hydrogen Energy 39: 10374–10379.
2. Si TZ, Pang G, Zhang QA, Liu DM, Liu N (2009) Solid solubility of Mg in Ca_2Ni_7 and hydrogen storage properties of $(Ca_{2-x}Mgx)Ni_7$ alloys. Int J Hydrogen Energy 34: 4833–4837.
3. Poletaev AA, Deny RV, Maehlen JP, Solberg JK, Tarasov BP, et al. (2012) Nanostructured rapidly solidified $LaMg_{11}Ni$ alloy: Microstructure, crystal structure and hydrogenation properties. Int J Hydrogen Energy. 37: 3548–3557.
4. Kohno T, Yoshida H, Kawashima F, Inaba T, Sakai I, et al. (2000) Hydrogen storage properties of new ternary system alloys: La_2MgNi_9, $La_5Mg_2Ni_{23}$, La_3MgNi_{14}. J Alloys Compd31: L5–L7.
5. Denys RV, Yartys VA, Sato M, Riabov AB, Delaplane RG (2007) Crystal chemistry and thermodynamic properties of anisotropic $Ce_2Ni_7H_{4.7}$ hydride. J Solid State Chem. 180: 2566–2576.
6. Nakamura J, Iwase K, Hayakawa H, Nakamura Y, Akiba E (2009) Structural study of La_4MgNi_{19} hydride by in situ X-ray and neutron powder diffraction. J Phys Chem C 113: 5853–5859.
7. Férey A, Cuevas F, Latroche M, Knosp B, Bernard P (2009) Elaboration and characterization of magnesium-substituted La_5Ni_{19} hydride forming alloys as active materials for negative electrode in Ni–MH battery. Electrochim Acta. 54: 1710–1714.
8. Liu ZY, Yan XL, Wang N, Chai YJ, Hou DL (2011) Cyclic stability and high rate discharge performance of $(La,Mg)_5Ni_{19}$ multiphase alloy. Int J Hydrogen Energy. 36: 4370–4374.
9. Kadir K, Sakai T, Uehara I (1997) Synthesis and structure determination of a new series of hydrogen storage alloys; RMg_2Ni_9 (R=La, Ce, Pr, Nd, Sm and Gd) built from $MgNi_2$ Laves-type layers alternating with AB_5 layers. J Alloys Compd 257: 115–121.
10. Denys RV, Yartys VA (2011) Effect of magnesium on the crystal structure and thermodynamics of the $La_{3-x}Mg_xNi_9$ hydrides. J Alloys Compd. 509S: S540–S548.
11. Kadir K, Sakai T, Uehara I (2000) Structural investigation and hydrogen storage capacity of $LaMg_2Ni_9$ and $(La_{0.65}Ca_{0.35})(Mg_{1.32}Ca_{0.68})Ni_9$ of the AB2C9 type structure. J Alloys Comp 02: 112–117.
12. Liu JJ, Han SM, Li Y, Yang SQ, Shen WZ, et al. An investigation on phase transformation and electrochemical properties of as-cast and annealed $La_{0.75}Mg_{0.25}Nix_{(x=3.0, 3.3, 3.5, 3.8)}$ alloys. J Alloys Comp 552: 119–126.

13. Lacher JR (1937) A theoretical formula for the solubility of hydrogen in palladium. Proceedings of the Royal Society of London. Series A, Mathematical and Physical Sciences (1934–1990). 161: 525–545.

14. Beeri O, Cohen D, Gavra Z, Johnson JR, Mintz MH (1998) High–pressure studies of the $Ti_1.8Cr_2$–H system Statistical thermodynamics above the critical temperature. J Alloys Comp 267: 113–120.

15. Beeri O, Cohen D, Gavra Z, Johnson JR, Mintz MH (2000) Thermodynamic characterization and statistical thermodynamics of the TiCrMn–H (D) system. J Alloys Compd 299: 217–226.

16. Beeri O, Cohen D, Gavra Z, Mintz MH (2003) Sites occupation and thermodynamic properties of the $TiCr_{2-x}Mn_x$–H_2 ($0 \le x \le 1$) system: statistical thermodynamics analysis. J Alloys Comp 352: 111–22.

17. Senoha H, Takeichia N, Yasudab K, Kiyobayashi T (2009) A theoretical interpretation of the pressure-composition isotherms of RNi5 (R = La, Pr, Nd and Sm) systems based on statistical mechanics. J Alloys Comp 470: 360–364.

18. Lexcellent C, Gondor G (2007) Analysis of hydride formation for hydrogen storage: Pressure-composition isotherm curves modeling. Intermetallics 15: 934–944.

19. Ledovskikh A, Danilov D, Rey WJJ, Notten PHL (2006) Modeling of hydrogen storage in hydride-forming materials: Statistical thermodynamics. Phys Rev B 73: 0141061–12.

20. Li Q, Chou KC, Lin Q, Jiang LJ, Zhan F (2004) Hydrogen absorption and desorption kinetics of Ag–Mg–Ni alloys. Int J Hydrogen Energy. 29: 843–8499.

21. Muthukumar P, Satheesh A, Linder M, Mertz R, Groll M (2009) Studies on hydriding kinetics of some La–based metal hydride alloys. Int J Hydrogen Energy. 34: 7253–7262.

22. Pourabdoli M, Raygan S , Abdizadeh H, Uner D (2013) Determination of kinetic parameters and hydrogen desorption characteristics of MgH2–10 wt% (9Ni–2Mg–Y) nano–composite. Int J Hydrogen Energy 38: 11910–11919.

23. Smith G, Goudy AJ (2001) Thermodynamics, kinetics and modeling studies of the LaNi52xCox hydride system. J Alloys Comp 316: 93–98.

24. Blanco MV, Borzone EM, Baruj A, Meyer GO (2014) Hydrogen sorption kinetics of La–Ni–Sn storage alloys. Int J Hydrogen Energy 39: 5858–5867.

25. Chou KC, Li Q, Lin Q, Jiang LJ, Xu KD (2005) Kinetics of absorption and desorption of hydrogen in alloy powder. Int J Hydrogen Energy 30: 301–309.

26. Chou KC, Xu KD (2007) A new model for hydriding and dehydriding reactions in intermetallics. Intermetallics 15: 767–77.

27. An XH, Li LG, Zhang JY, Li Q (2012) Comparison of dehydriding kinetics between pure $LaNi_5$ and its substituted systems. J Alloys Comp 511: 154–158.

28. Luo Q, An XH, Pan YB, Zhang X, Zhang JY, et al. (2010) The hydriding kinetics of MgeNi based hydrogen storage alloys: A comparative study on Chou model and Jander model. Int J Hydrogen Energy 35: 7842–7849.

29. Liu J, Zhang X, Li Q, Chou KC, Xu KD (2009) Investigation on kinetics mechanism of hydrogen absorption in the La_2Mg_{17}-based composites. Int J Hydrogen Energy 34: 1951–1957.

30. Chou KC, Luo Q, Li Q, Zhang JY (2014) Influence of the density of oxide on oxidation kinetics. Intermetallics 47: 17–22.

31. An XH, Wu KB, Zhang JY, Chen SL, Li Q (2013) Thermodynamic reassessment of the La–Mg–Ni system and its application to hydrogen storage system. TMS 2013 Annual Meeting Collected Proceedings 845–852.

32. Pilling NB, Member MS, Bedworth RE (1923) The oxidation of metals at high temperatures. J Inst Met 29: 529–591.

33. Carter, RE (1961) Kinetic model for solid-state reactions. J Chem Phys 34: 2010-2015.